AIMS Mathematics, 10(8): 17779–17800.
DOI: 10.3934/math.2025793
Received: 17 January 2025
Revised: 18 May 2025
Accepted: 20 May 2025
Published: 06 August 2025

https://www.aimspress.com/journal/Math

Research article

Investigating novel soliton solutions and chaotic Structures for the (3+1)-dimensional fractional q-deformed tanh-Gordon model

Ayesha Naseem and Rashida Hussain*

Department of Mathematics, Mirpur University of Science and Technology, Mirpur-10250 (AJK), Pakistan

* **Correspondence:** Email: drrashida@must.edu.pk.

Abstract: The generalized (3+1)-dimensional fractional q-deformed tanh-Gordon model and its optical solutions are studied under various physical conditions. Verifying our analytical findings and using the modified Sardar-sub equation technique (SSET) to examine the behavior of the governing model through convergence criteria under different parameters of the hyperbolic local derivative. By generating diverse optical phenomena and flexibility of the governing model, our findings pave the way for additional theoretical and applied physics research. The objective is also to study the bifurcation and chaotic behavior of the equation. To accomplish this, a dynamical system is created using the Galilean transformation. Analyzing the bifurcation and chaotic structure of the equation to identify important transitions that lead to chaotic behavior, and using phase-space analysis to understand the system's unpredictability. The study shows how small adjustments can have a significant effect on the results. This study clarifies the behavior of the model, which is crucial for several applications in quantum mechanics, physics, and optics.

Keywords: (3+1)-dimensional fractional q-deformed equation; hyperbolic local derivative; soliton solutions; SSET; bifurcation analysis; quasi-periodic chaotic structure; symbolic computation
Mathematics Subject Classification: 35Q51, 35C08, 37D45, 37G25

1. Introduction

The majority of phenomena observed in our universe are controlled by non-linear partial differential equations (NLPDEs) and find extensive applications across many complex scientific areas enforced in various disciplines such as optics [1–3], physics, biophysics, plasma physics, quantum mechanics, [4,5] fluid dynamics, [6] nuclear engineering, deep hydrodynamics, chemistry [7–9] and several others. Many researchers believe that the exact solution of NLPDEs is the most compelling and interesting scientific field these days. Different analytical methods have been employed to derive precise

solutions for NLPDEs, for instance, the sine–cosine technique [10], the sech-sech technique [11], the modified extended Fan sub-equation technique [12], the exp-function technique [13], the extended sech technique [14], the $(\frac{G'}{G})$-expansion technique [15], the $\exp(-\phi)$ expansion technique [16], the F-expansion technique [17], the Hirota's technique [18], the inverse scattering technique [19], the Darboux's technique [20], the modified Khater techniques [21], the Riccati-Bernoulli sub-ODE technique [22], and many others.

Both mathematicians and physicists have been captivated by the fascinating and potent family of mathematical constructions known as q-deformed models. These equations, which add a deformation parameter q, have become an essential tool for solving the puzzles of quantum systems and opening up new research directions in a variety of domains. An interesting interaction between quantum and classical mechanics is at the core of the q-deformed model. These equations smoothly connect the weird and amazing quantum world with the well-known Newtonian world by introducing the q-deformation [23]. These equations have transformed our knowledge of particles interactions in the field of quantum field theory, opening the door for creating ground-breaking theories like quantum groups and quantum algebras. These developments significantly impact our understanding of the underlying forces governing particles existence. Furthermore, there are several uses for q-deformed equations in fields as disparate as knot theory, statistical mechanics, and the analysis of integrable systems. These equations have opened up new possibilities for technological advancement in condensed matter physics by illuminating the behavior of exotic materials such as topological insulators [24].

Fractional and nonlinear differential equations have been used to simulate complicated physical systems, such as chaos and soliton dynamics, in recent publications like [25, 26]. These works show how sophisticated analytical techniques are becoming more and more important in applied mathematics. By using the SSET on a fractional q-deformed model, we develop new soliton solutions that may find use in plasma physics and nonlinear optics, furthering this avenue of inquiry. Eleuch [27] presented the generalized q-deformed sinh-Gordon equation. This equation is an expansion of the conventional sinh-Gordon equation.

$$\frac{\partial^2 R(x,t)}{\partial x^2} - \frac{\partial^2 R(x,t)}{\partial t^2} = \left[\sinh_q\left(R^\gamma\right)\right]^p - \delta, \quad t \geqslant 0, \quad 0 < q \leqslant 1, \tag{1.1}$$

where $\sinh_q$ is presented as:

$$\sinh_q(t) = \frac{\mathrm{e}^t - q\mathrm{e}^{-t}}{2}, \tag{1.2}$$

and $\cosh_q$ is presented as:

$$\cosh_q(t) = \frac{\mathrm{e}^t + q\mathrm{e}^{-t}}{2}. \tag{1.3}$$

This current work is novel, as it applies the SSET to a governing model. In contrast to previous research, we investigate a generalized model that combines q-deformation and fractional calculus, allowing for a more thorough comprehension of nonlinear wave patterns. The obtained solutions include dark, bright, periodic and singular solitons, along with a detailed bifurcation and chaos analysis, offering deeper insights into the system's dynamics. The technique is effective and straightforward and produces precise results, making it a useful substitute for more intricate or exclusively numerical methods. This adds to the expanding body of research on analytical techniques related to fractional nonlinear dynamics. Many researchers have conducted analytical and numerical

studies for (1.1) [27]. In 2023, Ali et al. revised the q-deformed sinh-Gordon equation [28]. The following is one way to write this new formulation:

$$\frac{\partial^2 R(x,t)}{\partial x^2} - \frac{\partial^2 R(x,t)}{\partial t^2} = \mathrm{e}^{\alpha R}\left[\sinh_q\left(R^{\gamma}\right)\right]^p - \delta. \tag{1.4}$$

The q-deformed equation was presented in a new version by Ali and Alharbi in 2024 [29]:

$$\frac{\partial^2 u(x,t)}{\partial x^2} - \frac{\partial^2 u(x,t)}{\partial t^2} = \left(\{\tanh_q u(x,t)^{\rho}\right)^p \left(\mathrm{e}^{\mathrm{viv}\, u(x,t)} + \beta q\right)^{\rho} - \delta, \tag{1.5}$$

where $\tanh_q$ is defined as:

$$\tanh_q(t) = \frac{\mathrm{e}^t + q\mathrm{e}^{-t}}{\mathrm{e}^t - q\mathrm{e}^{-t}}. \tag{1.6}$$

Fractional calculus and q-calculus, which both expand classical calculus to capture more complicated behaviors in physical systems, interact to provide the study of fractional q-deformed equations. The fractional derivative takes memory effects and anomalous diffusion into account, while the q-deformation adds a discrete or quantum parameter that alters the equation's fundamental symmetry. These kinds of models have drawn a lot of interest because of their use in complex media, quantum field theory, and nonlinear optics. Specifically, classical soliton models are generalized to more realistic settings where both nonlocal and nonclassical features are crucial when using the time-fractional q-deformed model. An analytical approach is used to analyze the solution's dynamics under deformation restrictions in [31], which recently reported soliton results pertaining to fractional q-deformed models. The (3+1)-dimensional fractional q-deformed tanh-Gordon model is presented in this study as follows [30]:

$$\frac{\partial^2 R(x,y,z,t)}{\partial x^2} + \lambda\frac{\partial^2 R(x,y,z,t)}{\partial y^2} + \mu\frac{\partial^2 R(x,y,z,t)}{\partial z^2} - \frac{\partial^{2\theta} R(x,y,z,t)}{\partial t^{2\theta}} = \left(tanh_q R(x,y,z,t)^l\right)^m \left(\mathrm{e}^{\alpha R(x,y,z,t)} + \beta q\right)^n - \delta. \tag{1.7}$$

The q-tanh function, represented as $\tanh_q$, is a characteristic of the governing equation, as $R(x,y,z,t)$ is scalar field. The constants $\lambda, \mu, \varrho, p, \alpha, \beta$, and ρ parameterize the equation, and the term δ denotes a source term. In addition to extending the standard q-deformed equation, this equation displays complex dynamical behavior and a wide range of nonlinear events. It is noteworthy that this specific equation, regarded as an extension of Eq (1.4), has never been presented before. It is important to highlight that although a similar version of this equation has previously been published in the literature [30], the version that is being offered here is a novel generalization in the fractional context that has never been documented. The SSET has become a potent technique in recent years for precisely solving nonlinear evolution equations, especially when dealing with fractional and deformed models. Because of its effectiveness in creating a range of solution structures, including bright, dark, kink, and singular solitons, this technique has been effectively applied to a number of physical models, including optical solitons. To the best of our knowledge, the current study is the first to apply the SSET to this particular formulation. Recent literature [30] has examined analogous equations with regard to Eq (1.7), which represents a fractional q-deformed model. Our main goal is to find new soliton structures and investigate the effects of the deformation parameter and the fractional order on the physical behavior of the solutions.

In this research, we thoroughly analyze the governing model of [30] and expand this model into fractional order. The particular extension derived here from Eq (1.4), with its unique form and application context, has not been reported before, despite the fact that structurally similar forms of Eq (1.7) can be found in the literature [30]. We use the novel SSET to provide accurate analytical solutions and solve the equation numerically using the correct SSET.

Our goal in this research is to use the SSET to precisely solve the governing equations. The SSET is used in this work to solve the fractional q-deformed problem. Although there are other methods, including Adomian decomposition and the homotopy perturbation method (HPM), the SSET was chosen because it is straightforward in offering precise solutions to fractional and nonlinear equations. The approach has proven successful in dealing with intricate models such as the one under study, and it enables us to derive explicit soliton solutions without the need for computationally costly numerical techniques or approximations. The derivative is easier to use in analytical calculations than traditional fractional derivatives like Caputo or Riemann-Liouville because it maintains the Leibniz, chain, and product rules in a form that is similar to the classical derivative. Additionally, it makes it simpler to reduce fractional partial differential equations (FPDEs) to ODEs, which is necessary for bifurcation analysis and the construction of accurate solutions like solitons. Because of this, the derivative is especially well-suited for nonlinear analysis and physical modeling in the context of fractional q-deformed systems. Additionally, we will attempt to investigate Eq (1.1) for bifurcation and chaotic analysis. We investigate the dynamical properties of the converted system and obtain two ODEs using Galilean transformation. Among these traits are the ideas of chaotic analysis and the bifurcation phenomena.

1.1. Hyperbolic local derivative

Fractional local derivatives play a significant role in scientific research. A novel class of fractional local derivatives, the hyperbolic local derivative, was very recently introduced. The notion and salient features of a novel fractional derivative are examined, $D^{\theta}_{hyp}u(t)$, which is an expansion to a conventional order derivative $\frac{du(t)}{dt}$.

Definition. Let $\theta = (0, 1)$ and $t > 0$, define

$$D^{\theta}_{hyp}u(t) = \lim_{\epsilon \to 0} \frac{u(t + \epsilon t^{\frac{1-\theta}{2}} sech((1-\theta)t^{\frac{1+\theta}{2}})) - u(t)}{\epsilon}.$$

Where u is a real valued function defined on $[a, b]$ and is θ-differentiable if

$$D^{\theta}_{hyp}u(a) = \lim_{t \to a^{+}} D^{\theta}_{hyp}u(t),$$

providing that $\lim_{t \to a^{+}} D^{\theta}_{hyp}u(t)$ exists.

Properties. Let $\theta = (0, 1]$, $\phi \in \mathfrak{R}^{+}$ and let u, v be θ-differentiable, then

$$D^{\theta}_{hyp}(c_1u + c_2v)(t) = c_1D^{\theta}_{hyp}u(t) + c_2D^{\theta}_{hyp}v(t), c_1, c_2 \in \mathfrak{R},$$
$$D^{\theta}_{hyp}(u.v)(t) = u(t).D^{\theta}_{hyp}v(t) + v(t).D^{\theta}_{hyp}u(t),$$

$$D^{\theta}_{hyp}\frac{u}{v}(t) = \frac{v(t).D^{\theta}_{hyp}u(t) - u(t).D^{\theta}_{hyp}v(t)}{v^2(t)},$$
$$D^{\theta}_{hyp}(\psi) = 0, \psi \in \Re,$$
$$D^{\theta}_{hyp}u(t) = t^{\frac{1-\theta}{2}} sech((1-\theta)t^{\frac{1+\theta}{2}})u'(t), u \in C^1,$$
$$D^{\theta}_{hyp}(t^{\varrho}) = \varrho t^{\frac{2\varrho-\theta-1}{2}} sech((1-\theta)t^{\frac{1+\theta}{2}}), \varrho \in \Re.$$

1.2. Convergence analysis

To prove that the governing model converges to the exact series, consider the following theorem.

Statement.

Assume B $\subset$ R is a Banach space with suitable ||.|| in which the sequence $w_q(x, t)$ is defined for a definite value of h, for a constant L $\in$ R. If $\left\|w_{q+1}(\psi, t)\right\| \leq \left\|w_q(\psi, t)\right\| \forall q$, then the series solution $w(\kappa, t) = \sum_{q=0}^{\infty} w_q(\psi, t)p^q$ converges absolutely to $w(\kappa, t) = L\sum_{q=0}^{\infty} w_q(\kappa, t)$.

Proof. By implying the ratio test of the power series, if A_l is a sequence of partial sums of the series $w(\psi, t) = \sum_{q=0}^{\infty} w_q(\psi, t)$, we want to prove that A_ℓ is a Cauchy sequence in B. Consider

$$\|A_{\ell+1}(\varkappa, t) - A_l(\kappa, t)\| = \|w_{\ell+1}(\kappa, t)\| \leq L\|w_l(\kappa, t)\| \leq L^2\|w_{\ell-1}(\kappa, t)\| \ldots \leq L^{\ell+1}\|w_0(\kappa, t)\|.$$

The paper's organization is as follows: In Section 2, we will discuss the methodology of the SSET. In Section 3, the implementation of the proposed method and the results acquired with the help of fractional hyperbolic local derivative are executed. Section 4 discusses the dynamic behavior to explore bifurcation and chaotic analysis. In Section 5, we will discuss the graphic representation of some of the achieved solutions and compare the analytical results with numerical results. Section 6 provides the conclusions of the work.

2. General description of the proposed method

This section aims to introduce the algorithm for the SSET which is employed to derive solutions for the equations. The following section describes the main steps of the method. We suppose the following fractional nonlinear partial differential equation (FNLPDE)

$$D^{\alpha}\Re(R, R_x, R_y, R_t, R_{xy}, R_{tz}, R_{xz}, R_{xt}, ...) = 0, \tag{2.1}$$

where $R = R(x, y, z, t)$, which is the unknown function and $\Re$ is a polynomial in $D^{\alpha}R(x, y, z, t)$ and its partial derivatives with respect to x, y, z *and* t.

Step 1. Using the traveling wave transformation

$$R(x, y, z, t) = R(\zeta), \quad \zeta = x + \epsilon y + \gamma z - \frac{2k}{1-\theta^2}\sinh\left((1-\theta)\Omega t^{\frac{1+\theta}{2}}\right), \tag{2.2}$$

into Eq (2.1), we obtain the following ODE

$$\mathcal{Z}(R, R', R'', R''', ...) = 0, \tag{2.3}$$

where $R = R(\zeta)$, $\frac{dR}{d\zeta} = R'$, $\frac{d^2R}{d\zeta^2} = R''$....

Step 2. The solution of Eq (2.3) has the following form:

$$R(\zeta) = \sum_{j=0}^{K} \rho_j \Theta^j(\zeta), \tag{2.4}$$

where ρ_j (j=0,1,2,...K) are the coefficients to be calculated, such that $\rho_K \neq 0$ and $\Theta(\zeta)$ satisfy the ODE in the form:

$$(\Theta'(\zeta))^2 = \nu + \alpha\Theta^2(\zeta) + \Theta^4(\zeta), \tag{2.5}$$

where ν and α are real constants.

Step 3. By the balancing principle, equating the nonlinear terms with the highest-order derivatives, we determine a positive integer K in Eq (2.4).

Step 4. By substituting Eqs (2.4) and (2.5) into Eq (2.3), we derive an equation involving powers of $\Theta(\zeta)$. Then collect all terms with the same powers of $\Theta^j(\zeta)$ (where j=0,1,2,...K) and set them equal to zero. This process yields a system of algebraic equations. Solving this system provides us with the values of ρ_j, ν, and α, and the solutions to Eq (1.1) are as follows:

Case I: If $\alpha > 0$, $\nu = 0$, then

$$\Theta_1^{\pm}(\zeta) = \pm\sqrt{-pq\alpha}\,\mathrm{sech}_{pq}\left(\sqrt{\alpha}\zeta\right),$$
$$\Theta_2^{\pm}(\zeta) = \pm\sqrt{pq\alpha}\,\mathrm{csch}_{pq}\left(\sqrt{\alpha}\zeta\right),$$

where

$$\mathrm{sech}_{pq}(\zeta) = \frac{2}{pe^{\zeta} + qe^{-\zeta}}, \quad \mathrm{csch}_{pq}(\zeta) = \frac{2}{pe^{\zeta} - qe^{-\zeta}}.$$

Case II: If $\alpha < 0$, $\nu = 0$, then

$$\Theta_3^{\pm}(\zeta) = \pm\sqrt{-pq\alpha}\,\mathrm{sec}_{pq}\left(\sqrt{-\alpha}\zeta\right),$$
$$\Theta_4^{\pm}(\zeta) = \pm\sqrt{-pq\alpha}\,\mathrm{csc}_{pq}\left(\sqrt{-\alpha}\zeta\right),$$

where

$$\mathrm{sec}_{pq}(\zeta) = \frac{2}{pe^{i\zeta} + qe^{-i\zeta}}, \quad \mathrm{csc}_{pq}(\zeta) = \frac{2}{pe^{i\zeta} - qe^{-i\zeta}}.$$

Case III: If $\alpha < 0$, $\nu = \frac{\alpha^2}{4}$, then

$$\Theta_5^{\pm}(\zeta) = \pm\sqrt{\frac{-\alpha}{2}}\tanh_{pq}\left(\sqrt{\frac{-\alpha}{2}}\zeta\right),$$

$$\Theta_6^{\pm}\zeta) = \pm\sqrt{\frac{-\alpha}{2}}\coth_{pq}\left(\sqrt{\frac{-\alpha}{2}}\zeta\right),$$

$$\Theta_7^{\pm}(\zeta) = \pm\sqrt{\frac{-\alpha}{2}}\left(\tanh_{pq}\left(\sqrt{-2\alpha}\zeta\right) \pm i\sqrt{pq}\,\mathrm{sech}_{pq}\left(\sqrt{-2\alpha}\zeta\right)\right),$$

$$\Theta_8^{\pm}(\zeta) = \pm\sqrt{\frac{-\alpha}{2}}\left(\coth_{pq}\left(\sqrt{-2\alpha}\zeta\right) \pm \sqrt{pq}\,\mathrm{csch}_{pq}\left(\sqrt{-2\alpha}\zeta\right)\right),$$

$$\Theta_9^{\pm}(\zeta) = \pm\sqrt{\frac{-\alpha}{2}}\left(\tanh_{pq}\left(\sqrt{\frac{-\alpha}{8}}\zeta\right) + \coth_{pq}\left(\sqrt{\frac{-\alpha}{8}}\zeta\right)\right),$$

where

$$\tanh_{pq}(\zeta) = \frac{p\mathrm{e}^{\zeta} - q\mathrm{e}^{-\zeta}}{p\mathrm{e}^{\zeta} + q\mathrm{e}^{-\zeta}}, \quad \coth_{pq}(\zeta) = \frac{p\mathrm{e}^{\zeta} + q\mathrm{e}^{-\zeta}}{p\mathrm{e}^{\zeta} - q\mathrm{e}^{-\zeta}}.$$

Case IV: If $\alpha > 0$, $\nu = \frac{\alpha^2}{4}$, then

$$\Theta_{10}^{\pm}(\zeta) = \pm\sqrt{\frac{\alpha}{2}}\tan_{pq}\left(\sqrt{\frac{\alpha}{2}}\zeta\right),$$

$$\Theta_{11}^{\pm}(\zeta) = \pm\sqrt{\frac{\alpha}{2}}\cot_{pq}\left(\sqrt{\frac{\alpha}{2}}\zeta\right),$$

$$\Theta_{12}^{\pm}(\zeta) = \pm\sqrt{\frac{\alpha}{2}}\left(\tan_{pq}\left(\sqrt{2\alpha}\zeta\right) \pm \sqrt{pq}\,\sec_{pq}\left(\sqrt{2\alpha}\zeta\right)\right),$$

$$\Theta_{13}^{\pm}(\zeta) = \pm\sqrt{\frac{\alpha}{2}}\left(\cot_{pq}\left(\sqrt{2\alpha}\zeta\right) \pm \sqrt{pq}\,\csc_{pq}\left(\sqrt{2\alpha}\zeta\right)\right),$$

$$\Theta_{14}^{\pm}(\zeta) = \pm\sqrt{\frac{\alpha}{2}}\left(\tan_{pq}\left(\sqrt{\frac{\alpha}{8}}\zeta\right) + \cot_{pq}\left(\sqrt{\frac{\alpha}{8}}\zeta\right)\right),$$

where

$$\tan_{pq}(\zeta) = -i\frac{p\mathrm{e}^{\zeta} - q\mathrm{e}^{-\zeta}}{p\mathrm{e}^{\zeta} + q\mathrm{e}^{-\zeta}}, \quad \cot_{pq}(\zeta) = i\frac{p\mathrm{e}^{\zeta} + q\mathrm{e}^{-\zeta}}{p\mathrm{e}^{\zeta} - q\mathrm{e}^{-\zeta}}.$$

Step 5. Utilizing the values of ρ_j, ν, and α and Eq (1.6) into Eq (1.5), we can obtain the exact solutions of Eq (1.2).

3. Implementation

3.1. Conversion of FNLPDEs into ODEs

In this subsection, determine the ODEs by using the fractional derivatives below.

$$R(x, y, z, t) = R(\zeta), \quad \zeta = x + \epsilon y + \gamma z - \frac{2k}{1-\theta^2}\sinh\left((1-\theta)\Omega t^{\frac{1+\theta}{2}}\right), \tag{3.1}$$

where k represents the speed of wave propagation. The fractional derivative of order α is defined as follows:

$$D_t^{\alpha} g(t) = \lim_{\varepsilon \to 0} \frac{g\left(t + \varepsilon t^{1-\alpha}\right) - g(t)}{\epsilon}, \quad \text{for all} \quad t > 0, \quad \alpha \in (0, 1). \tag{3.2}$$

The following are the properties of fractional derivatives:

(**1**) $D_t^{\alpha}\left(\alpha_1 g(t) + \beta_1 h(t)\right) = D_t^{\alpha} g(t) + D_t^{\alpha} h(t)$.
(**2**) $D_t^{\alpha}(c) = 0$.
(**3**) $D_t^{\alpha}\left(g(t)^* h(t)\right) = h(t) D_t^{\alpha} g(t) + g(t) D_t^{\alpha} h(t)$.
(**4**) $D_t^{\alpha}\left(\frac{g(t)}{h(t)}\right) = \frac{h(t) D_t^{\alpha} g(t) - g(t) D_t^{\alpha} h(t)}{h^2(t)}$,

where g and h are differentiable of order α at $t > 0$. By using Eq (3.1), Eq (1.7) becomes the required ODE.

$$\left(1 + \lambda\epsilon^2 + \mu\gamma^2 - k^2\right) R''[\zeta) - \left(tanh_q R(\zeta)^l\right)^m \left(\mathrm{e}^{\alpha R(\zeta)} + \beta q\right)^n + \delta = 0. \tag{3.3}$$

• Suppose $\alpha = 2,\ l = m = n = 1,\ \delta = -q,\ \beta = 1,\ a = 9,\ p = 1$.

Thus, Eq (3.3) can be rewritten as:

$$\left(1 + \lambda\epsilon^2 + \mu\gamma^2 - k^2\right) R''(\zeta) - \left(\mathrm{e}^{2R(\zeta)}\right) = 0. \tag{3.4}$$

We can multiply both sides of Eq (3.4) by $R'(\zeta)$ and get the following equation after integration:

$$\frac{1}{2}\left(-\left(1 + \lambda\epsilon^2 + \mu\gamma^2 - k^2\right) R'(\zeta)^2 - \mathrm{e}^{2R(\zeta)}\right) - C_1 = 0. \tag{3.5}$$

The integration constant is C_1. Let

$$R(\zeta) = \frac{1}{2}\ln(h(\zeta)). \tag{3.6}$$

Here, Eq (3.5) becomes

$$-8C_1 h(\zeta)^2 + \left(1 + \lambda\epsilon^2 + \mu\gamma^2 - k^2\right) h'(\zeta)^2 - 4h(\zeta)^3 = 0. \tag{3.7}$$

By homogeneous balancing principle to determine the value of the parameter K by balancing in Eq (3.7), we get $K = 2$. We can rewrite Eq (2.4) as follows:

$$h(\zeta) = \rho_0 + \rho_1 \Theta(\zeta) + \rho_2 \Theta^2(\zeta). \tag{3.8}$$

A system of algebraic equations is formed by substituting Eq (3.8) into Eq (3.7) with Eq (2.5) and then setting the coefficients of the corresponding powers of $\Theta^j(\zeta),\ (j = 0, 1, 2, ...)$ to zero.

$$\begin{aligned}
&\mu\gamma^2\nu\rho_1^2 - 8C_1\rho_0^2 - k^2\nu\rho_1^2 + \nu\rho_1^2 - 4\rho_0^3 + \nu\rho_1^2\lambda\epsilon^2 = 0,\\
&4\mu\gamma^2\nu\rho_1\rho_2 - 16C_1\rho_0\rho_1 - 4k^2\nu\rho_1\rho_2 + 4\nu\rho_1\rho_2 - 12\rho_0^2\rho_1 + 4\nu\rho_1\rho_2\lambda\epsilon^2 = 0,\\
&\alpha\mu\gamma^2\rho_1^2 + \alpha\rho_1^2 + \alpha\rho_1^2\lambda\epsilon^2 + 4\mu\gamma^2\nu\rho_2^2 - 16C_1\rho_2\rho_0 - 8C_1\rho_1^2 - \alpha k^2\rho_1^2 - 4k^2\nu\rho_2^2 + 4\nu\rho_2^2 - 12\rho_2\rho_0^2\\
&- 12\rho_1^2\rho_0 + 4\nu\rho_2^2\lambda\epsilon^2 = 0,
\end{aligned}$$

$4\alpha\mu\gamma^2\rho_2\rho_1 + 4\alpha\rho_2\rho_1 + 4\alpha\rho_2\rho_1\lambda\epsilon^2 - 16C_1\rho_2\rho_1 - 4\alpha k^2\rho_2\rho_1 - 4\rho_1^3 - 24\rho_0\rho_2\rho_1 = 0,$
$4\alpha\mu\gamma^2\rho_2^2 + 4\alpha\rho_2^2 + 4\alpha\rho_2^2\lambda\epsilon^2 + \mu\gamma^2\rho_1^2 - 8C_1\rho_2^2 - 4\alpha k^2\rho_2^2 - k^2\rho_1^2 - 12\rho_2\rho_1^2 + \rho_1^2 - 12\rho_0\rho_2^2 + \rho_1^2\lambda\epsilon^2 = 0,$
$4\mu\gamma^2\rho_1\rho_2 - 4k^2\rho_1\rho_2 - 12\rho_1\rho_2^2 + 4\rho_1\rho_2 + 4\rho_1\rho_2\lambda\epsilon^2 = 0,$
$4\mu\gamma^2\rho_2^2 - 4k^2\rho_2^2 - 4\rho_2^3 + 4\rho_2^2 + 4\rho_2^2\lambda\epsilon^2 = 0.$

After solving this system of equations for $\{\rho_0, \rho_1, \rho_2, \nu, k, \alpha\}$, we obtain

$$\rho_1 = 0, \ \ \rho_0 = -2C_1, \ \ \alpha = -\frac{4C_1}{\rho_2}, \ \ \nu = \frac{4C_1^2}{\rho_2^2}, \ \ k = \sqrt{\mu\gamma^2 - \rho_2 + \lambda\epsilon^2 + 1}. \tag{3.9}$$

Now derive the exact soliton solutions for Eq (1.1).

3.2. Wave solutions

Case I: If $\alpha > 0$, $\nu = 0$, then

$$R_1^{\pm}(x,y,z,t) = \frac{1}{2}\log\left(\rho_2\left(\pm\left(2\sqrt{\frac{C_1pq}{\rho_2}}\right)\right)^2 sech_{pq}\left(2\sqrt{-\frac{C_1}{\rho_2}}\left(\frac{\rho_2\sqrt{\mu\gamma^2-\rho_2+\lambda\epsilon^2+1}t^{-\frac{4C_1}{\rho_2}}}{4C_1} + x + y + z\right)\right)^2 - 2C_1\right), \tag{3.10}$$

$$R_2^{\pm}(x,y,z,t) = \tfrac{1}{2}\log\left(\rho_2\left(\pm\left(2\sqrt{-\frac{C_1pq}{\rho_2}}\right)\right)^2 csch_{pq}\left(2\sqrt{-\frac{C_1}{\rho_2}}\left(\frac{\rho_2\sqrt{\mu\gamma^2-\rho_2+\lambda\epsilon^2+1}t^{-\frac{4C_1}{\rho_2}}}{4C_1} + x + y + z\right)\right)^2 - 2C_1\right). \tag{3.11}$$

Case II: If $\alpha < 0$, $\nu = 0$, then

$$R_3^{\pm}(x,y,z,t) = \tfrac{1}{2}\log\left(\rho_2\left(\pm\left(2\sqrt{\frac{C_1pq}{\rho_2}}\right)\right)^2 sec_{pq}\left(2\sqrt{\frac{C_1}{\rho_2}}\left(\frac{\rho_2\sqrt{\mu\gamma^2-\rho_2+\lambda\epsilon^2+1}t^{-\frac{4C_1}{\rho_2}}}{4C_1} + x + y + z\right)\right)^2 - 2C_1\right), \tag{3.12}$$

$$R_4^{\pm}(x,y,z,t) = \tfrac{1}{2}\log\left(\rho_2\left(\pm\left(2\sqrt{\frac{C_1pq}{\rho_2}}\right)\right)^2 csc_{pq}\left(2\sqrt{\frac{C_1}{\rho_2}}\left(\frac{\rho_2\sqrt{\mu\gamma^2-\rho_2+\lambda\epsilon^2+1}t^{-\frac{4C_1}{\rho_2}}}{4C_1} + x + y + z\right)\right)^2 - 2C_1\right). \tag{3.13}$$

Case III: If $\alpha < 0$, $\nu = \frac{\alpha^2}{4}$, then

$$R_5^{\pm}(x,y,z,t) = \tfrac{1}{2}\log\left(\rho_2\left(\pm\left(\sqrt{2}\sqrt{\frac{C_1}{\rho_2}}\right)\right)^2 tanh_{pq}\left(\sqrt{2}\sqrt{\frac{C_1}{\rho_2}}\left(\frac{\rho_2\sqrt{\mu\gamma^2-\rho_2+\lambda\epsilon^2+1}t^{-\frac{4C_1}{\rho_2}}}{4C_1} + x + y + z\right)\right)^2 - 2C_1\right), \tag{3.14}$$

$$R_6^{\pm}(x,y,z,t) = \tfrac{1}{2}\log\left(\rho_2\left(\pm\left(\sqrt{2}\sqrt{\frac{C_1}{\rho_2}}\right)\right)^2 coth_{pq}\left(\sqrt{2}\sqrt{\frac{C_1}{\rho_2}}\left(\frac{\rho_2\sqrt{\mu\gamma^2-\rho_2+\lambda\epsilon^2+1}t^{-\frac{4C_1}{\rho_2}}}{4C_1} + x + y + z\right)\right)^2 - 2C_1\right), \tag{3.15}$$

$$R_7^{\pm}(x,y,z,t) = \frac{1}{2}\log\left(-2C_1 + \rho_2\left(\pm\left(\sqrt{2}\sqrt{\frac{C_1}{\rho_2}}\right)\right)^2\right.$$

$$\times\left[\tanh_{pq}\left(2\sqrt{2}\sqrt{\frac{C_1}{\rho_2}}\left(\frac{\rho_2\sqrt{\mu\gamma^2-\rho_2+\lambda\epsilon^2+1}\,t^{-\frac{4C_1}{\rho_2}}}{4C_1}+x+y+z\right)\right)\right.$$
$$\left.\pm i\sqrt{pq}\,sech_{pq}\left(2\sqrt{2}\sqrt{\frac{C_1}{\rho_2}}\left(\frac{\rho_2\sqrt{\mu\gamma^2-\rho_2+\lambda\epsilon^2+1}\,t^{-\frac{4C_1}{\rho_2}}}{4C_1}+x+y+z\right)\right)\right]^2\Bigg) \tag{3.16}$$

$$R_8^{\pm}(x,y,z,t)=\frac{1}{2}\log\left(\rho_2\left(\pm\sqrt{2}\sqrt{\frac{C_1}{\rho_2}}\right)^2\left[coth_{pq}\left(2\sqrt{2}\sqrt{\frac{C_1}{\rho_2}}\left(\frac{\rho_2\sqrt{\mu\gamma^2-\rho_2+\lambda\epsilon^2+1}\,t^{-\frac{4C_1}{\rho_2}}}{4C_1}+x+y+z\right)\right)\right.\right.$$
$$\left.\left.\pm\sqrt{pq}\,csch_{pq}\left(2\sqrt{2}\sqrt{\frac{C_1}{\rho_2}}\left(\frac{\rho_2\sqrt{\mu\gamma^2-\rho_2+\lambda\epsilon^2+1}\,t^{-\frac{4C_1}{\rho_2}}}{4C_1}+x+y+z\right)\right)\right]^2-2C_1\right) \tag{3.17}$$

$$R_9^{\pm}(x,y,z,t)=\frac{1}{2}\log\left(\rho_2\left(\pm\frac{\sqrt{\frac{C_1}{\rho_2}}}{\sqrt{2}}\right)^2\left[coth_{pq}\left(\frac{\sqrt{\frac{C_1}{\rho_2}}}{\sqrt{2}}\left(\frac{\rho_2\sqrt{\mu\gamma^2-\rho_2+\lambda\epsilon^2+1}\,t^{-\frac{4C_1}{\rho_2}}}{4C_1}+x+y+z\right)\right)\right.\right.$$
$$\left.\left.+tanh_{pq}\left(\frac{\sqrt{\frac{C_1}{\rho_2}}}{\sqrt{2}}\left(\frac{\rho_2\sqrt{\mu\gamma^2-\rho_2+\lambda\epsilon^2+1}\,t^{-\frac{4C_1}{\rho_2}}}{4C_1}+x+y+z\right)\right)\right]^2-2C_1\right) \tag{3.18}$$

Case IV: If $\alpha>0$, $\nu=\frac{\alpha^2}{4}$, then

$$R_{10}^{\pm}(x,y,z,t)=\tfrac{1}{2}\log\left(\rho_2\left(\pm\left(\sqrt{2}\sqrt{-\tfrac{C_1}{\rho_2}}\right)\right)^2 tan_{pq}\left(\sqrt{2}\sqrt{-\tfrac{C_1}{\rho_2}}\left(\frac{\rho_2\sqrt{\mu\gamma^2-\rho_2+\lambda\epsilon^2+1}\,t^{-\frac{4C_1}{\rho_2}}}{4C_1}+x+y+z\right)\right)^2-2C_1\right), \tag{3.19}$$

$$R_{11}^{\pm}(x,y,z,t)=\tfrac{1}{2}\log\left(\rho_2\left(\pm\left(\sqrt{2}\sqrt{-\tfrac{C_1}{\rho_2}}\right)\right)^2 cot_{pq}\left(\sqrt{2}\sqrt{-\tfrac{C_1}{\rho_2}}\left(\frac{\rho_2\sqrt{\mu\gamma^2-\rho_2+\lambda\epsilon^2+1}\,t^{-\frac{4C_1}{\rho_2}}}{4C_1}+x+y+z\right)\right)^2-2C_1\right), \tag{3.20}$$

$$R_{12}^{\pm}(x,y,z,t)=\frac{1}{2}\log\left(\rho_2\left(\pm\sqrt{2}\sqrt{-\frac{C_1}{\rho_2}}\right)^2\left[tan_{pq}\left(2\sqrt{2}\sqrt{-\frac{C_1}{\rho_2}}\left(\frac{\rho_2\sqrt{\mu\gamma^2-\rho_2+\lambda\epsilon^2+1}\,t^{-\frac{4C_1}{\rho_2}}}{4C_1}+x+y+z\right)\right)\right.\right.$$
$$\left.\left.\pm\sqrt{pq}sec_{pq}\left(2\sqrt{2}\sqrt{-\frac{C_1}{\rho_2}}\left(\frac{\rho_2\sqrt{\mu\gamma^2-\rho_2+\lambda\epsilon^2+1}\,t^{-\frac{4C_1}{\rho_2}}}{4C_1}+x+y+z\right)\right)\right]^2-2C_1\right), \tag{3.21}$$

$$R_{13}^{\pm}(x,y,z,t)=\frac{1}{2}\log\left(\rho_2\left(\pm\sqrt{2}\sqrt{-\frac{C_1}{\rho_2}}\right)^2\left[cot_{pq}\left(2\sqrt{2}\sqrt{-\frac{C_1}{\rho_2}}\left(\frac{\rho_2\sqrt{\mu\gamma^2-\rho_2+\lambda\epsilon^2+1}\,t^{-\frac{4C_1}{\rho_2}}}{4C_1}+x+y+z\right)\right)\right.\right.$$

$$\pm \sqrt{pq}csc_{pq}\left(2\sqrt{2}\sqrt{-\frac{C_1}{\rho_2}}\left(\frac{\rho_2\sqrt{\mu\gamma^2-\rho_2+\lambda\epsilon^2+1}\,t^{-\frac{4C_1}{\rho_2}}}{4C_1}+x+y+z\right)\right)\Bigg]^2-2C_1\Bigg), \tag{3.22}$$

$$R_{14}^{\pm}(x,y,z,t)=\frac{1}{2}\log\Bigg(\rho_2\left(\pm\frac{\sqrt{-\frac{C_1}{\rho_2}}}{\sqrt{2}}\right)^2\Bigg[cot_{pq}\left(\frac{\sqrt{-\frac{C_1}{\rho_2}}}{\sqrt{2}}\left(\frac{\rho_2\sqrt{\mu\gamma^2-\rho_2+\lambda\epsilon^2+1}\,t^{-\frac{4C_1}{\rho_2}}}{4C_1}+x+y+z\right)\right)$$
$$+tan_{pq}\left(\frac{\sqrt{-\frac{C_1}{\rho_2}}}{\sqrt{2}}\left(\frac{\rho_2\sqrt{\mu\gamma^2-\rho_2+\lambda\epsilon^2+1}\,t^{-\frac{4C_1}{\rho_2}}}{4C_1}+x+y+z\right)\right)\Bigg]^2-2C_1\Bigg). \tag{3.23}$$

4. Explorations of bifurcation and chaotic analysis of the governing equation

In this section, we explore bifurcation and chaotic analysis. The primary objective of this section is to convert Eq (3.7) into planar dynamic systems by utilizing Galilean transformation. We then explore the bifurcation and chaos of the governing equation.

4.1. Dynamic system

Using Galilean transformation, we simplify an ODE into a planar dynamic system. This transformation reduces the number of independent variables by reducing their relative position or simplifying their relationships. For instance, we reduced a model with two spatial and one temporal variable to a system of equations that only depend on time. Considering Eq (3.7), its derivative concerning time evolution can be written as

$$-8C_1h(\zeta)+\left(1+\lambda\epsilon^2+\mu\gamma^2-k^2\right)h''(\zeta)-6h(\zeta)^2=0. \tag{4.1}$$

Let $h'(\zeta)=Z_1$. Then the dynamic system of Eq (4.1) is described as follows:

$$\begin{cases}\frac{dh(\zeta)}{d\zeta} &= Z_1=N,\\ \frac{dZ_1(\zeta)}{d\zeta} &= B_1h(\zeta)+B_2h^2(\zeta)=G,\end{cases} \tag{4.2}$$

where $B_1=\frac{8C_1}{(1+\lambda\epsilon^2+\mu\gamma^2-k^2)}$ and $B_2=\frac{6}{(1+\lambda\epsilon^2+\mu\gamma^2-k^2)}$. The reduced form of Eq (4.2), makes bifurcation and phase plane analysis easier. This method has been hypothetically tested and is consistent with traditional approaches in nonlinear dynamics.

4.2. Bifurcation analysis

Bifurcation refers to sudden changes in a system's dynamics caused by varying parameters [36–38]. Bifurcation analysis can explain variations in ocean wave formation patterns, including changes in wave speed and wavelength. By studying bifurcation processes, we can forecast and explain waves

behavior under various parameter settings. This provides a framework for ocean wave simulation and prediction. Now we solve the system to find the equilibrium points of Eq (4.2).

$$\begin{cases} N = 0, \\ G = 0. \end{cases}$$

Thus the equilibrium points are

$$\mathcal{M}_1 = (-\frac{B_1}{B_2}, 0), \quad \mathcal{M}_2 = (0, 0).$$

To obtain the determinant of the system (4.2), we use

$$\boldsymbol{J}(N, G) = \begin{vmatrix} 0 & 1 \\ B_1 + 2B_2h(\zeta) & 0 \end{vmatrix} = -(B_1 + 2B_2h).$$

Equilibrium points are crucial to determining phase orbit behavior. We note the following:

- When $\boldsymbol{J}(N, G) < 0$, then (N, G) behaves as saddle point.
- When $\boldsymbol{J}(N, G) > 0$, then (N, G) behaves as center point.
- When $\boldsymbol{J}(N, G) = 0$, then (N, G) behaves as a cuspidal point.

To analyze the system (4.2) via a phase portrait point of view, we examine changes in the bifurcation behavior as the parameters vary. We can understand the impact of bifurcation by visualizing the system's phase portrait for different parameter configurations. This comprehensive analysis of various parameter settings enables us to gain a better understanding of the system's dynamics and evolving behavior.

The results that can be obtained by changing the relevant parameter are given here.

Case I: When $B_1 > 0$ and $B_2 > 0$

By setting the specific parameter values $\epsilon = 1, C_1 = 1, \lambda = 1, \mu = 1, k = 1$ and $\gamma = 1$, we obtain equilibrium points (-1.33,0) and (0,0) as represented in Figure 1(a), in which (0,0) behaves as saddle point and (-1.33,0) act as center point.

Case II: When $B_1 < 0$ and $B_2 > 0$

By setting the specific parameter values $\epsilon = 1, C_1 = -1, \lambda = 1, \mu = 1, k = 1$ and $\gamma = -1$ we get equilibrium points (0,0) and (1.33,0) which are visualized in Figure 1(b). Clearly (0,0) represents a center and (1.33,0) is saddle point.

Case III: When $B_1 > 0$ and $B_2 < 0$

By setting the specific parameter values $\epsilon = 1, C_1 = -1, \lambda = 1, \mu = 1, k = 2$ and $\gamma = 1$, we observe equilibrium point (0,0) and (1.33,0), which is illustrated in Figure 2(a). Evidently, (0,0) represents a saddle point and (1.33,0) is center.

Case IV: When $B_1 < 0$ and $B_2 < 0$

By setting the specific parameter values $\epsilon = 1, C_1 = 1, \lambda = 1, \mu = 1, k = 2,$ and $\gamma = 1$, we get equilibrium points (-1.33,0) and (0,0)as depicted in Figure 2(b), in which (0,0) behaves as a center point, (-1.33,0) act as saddle point.

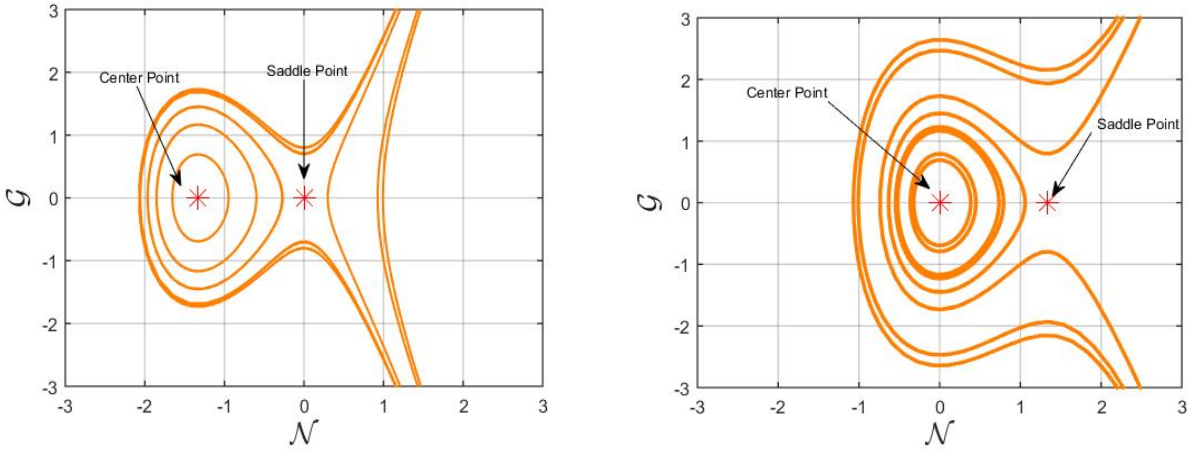

(a) (b)

Figure 1. Phase portraits for Case I and Case II are represented in Figure (a),(b) respectively. In both figures star symbol depicts the equilibrium point.

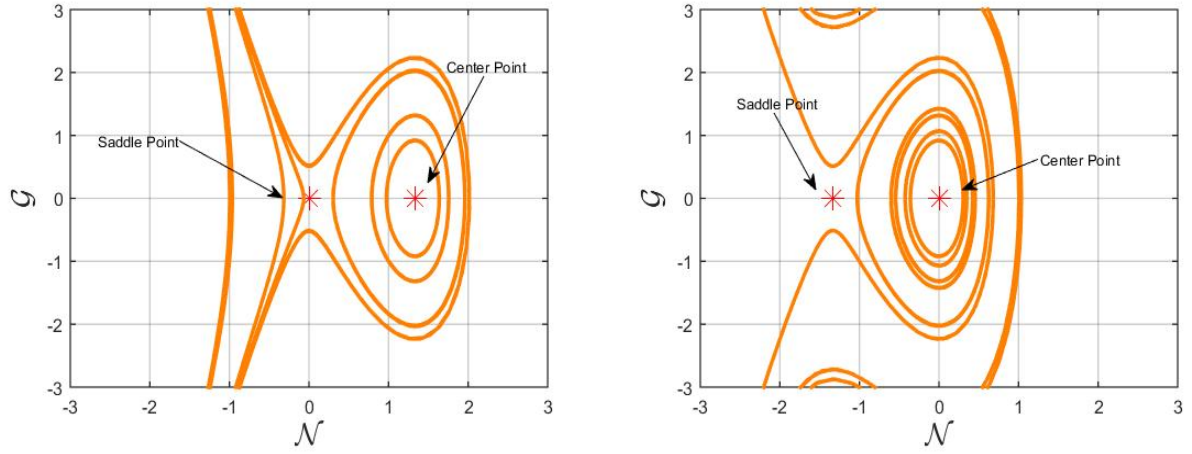

(a) (b)

Figure 2. Figure (a),(b) Phase portraits for Case III and Case IV, respectively. In both figures star symbol depicts the equilibrium point.

4.3. Chaotic behavior

In this subsection, we investigate the quasi-periodic chaotic [32–35] behavior exhibited by the system Eq (3.17) when a perturbation term is introduced. To provide a clearer understanding of the system's chaotic nature, we present both two- and three-dimensional phase diagrams. The dynamical system resulting from the perturbation of system Eq (4.2) is expressed as follows:

$$\begin{cases} \frac{dh(\zeta)}{d\zeta} & = Z_1 = N, \\ \frac{dZ_1(\zeta)}{d\zeta} & = B_1 h(\zeta) + B_2 h^2(\zeta) + \hat{\alpha}\cos(\varepsilon t) = G. \end{cases} \tag{4.3}$$

Our focus is on examining how the frequency ε and amplitude $\hat{\alpha}$ in the perturbation term $\hat{\alpha}\cos(\varepsilon t)$ influence the system's dynamics. Figures 3 and 4 depict the behavior of the system in Eq (4.3) under various values of $\hat{\alpha}$ and ε, while keeping the other parameters as: $C_1 = -0.7$, $K = 0.5$, $\epsilon = 2.0$, $\gamma = 0.5$, $\lambda = 1$ and $\mu = 1$. In Figure 3(a),(b), where $\hat{\alpha}$ and ε are set to 0.05 and 0.09, respectively, relatively simple, spiral-like pattern is observed. In Figure 4(a),(b), with $\hat{\alpha}$ and ε set to 0.09 and 0.1, we see a more symmetrical but still chaotic pattern. Moreover, in Figure 5(a),(b) and Figure 6(a),(b), where $\hat{\alpha}$ and ε are set as (0.1, 0.25) and (0.2, 0.25) respectively, we observe the system displays a relatively a complex, spiral structure. These visualizations highlight how changes in the parameters $\hat{\alpha}$ and ε affect the chaotic behavior of the system, leading to a range of complex and unpredictable patterns. The visualizations provided here effectively demonstrate the chaotic nature of the perturbed dynamic system. If we set the fractional order equal to 1, the systems turn into their classic form, but when $0 < \alpha < 1$, the memory and hereditary effects introduced by the fractional operator change the qualitative behavior of the system. This effect manifests in the phase portraits and bifurcation patterns, which are significantly different from the case of classical systems. The motivation for employing the fractional derivative therefore, lies in the ability to capture these intricate dynamic properties that are not present in the integer-order systems.

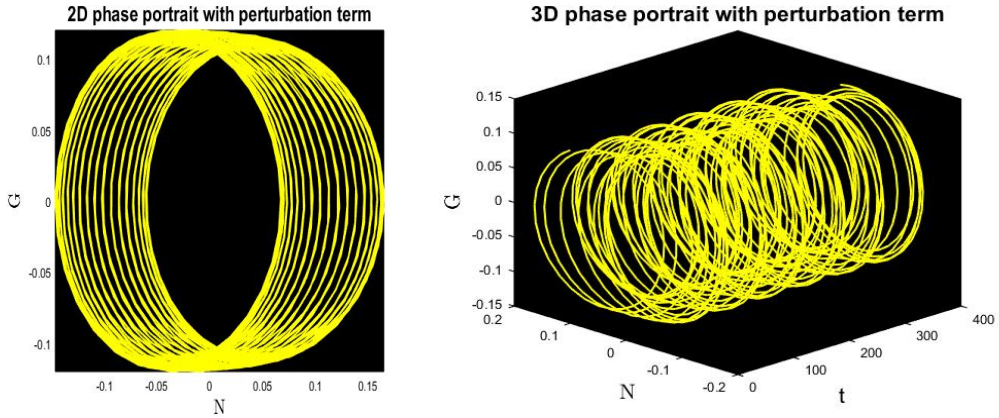

(a) (b)

Figure 3. Visualization of 2D and 3D chaotic dynamics with $\hat{\alpha} = 0.05$ and $\varepsilon = 0.09$.

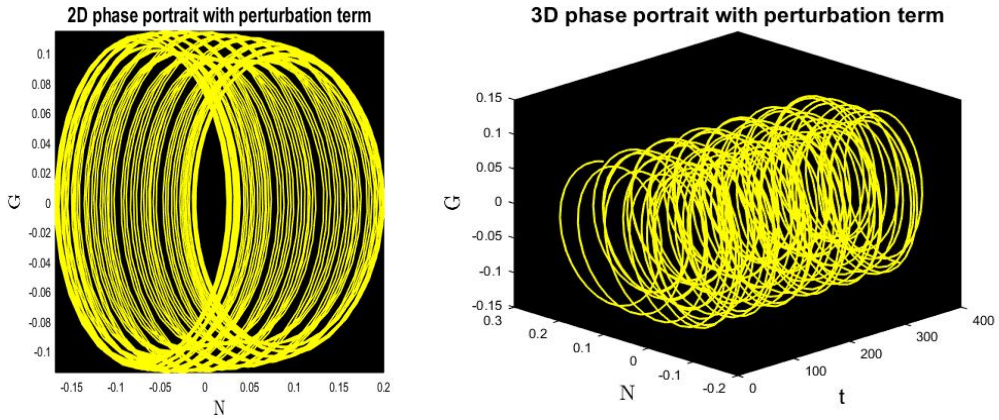

(a) (b)

Figure 4. Visualization of 2D and 3D chaotic dynamics with $\hat{\alpha} = 0.09$ and $\varepsilon = 0.1$.

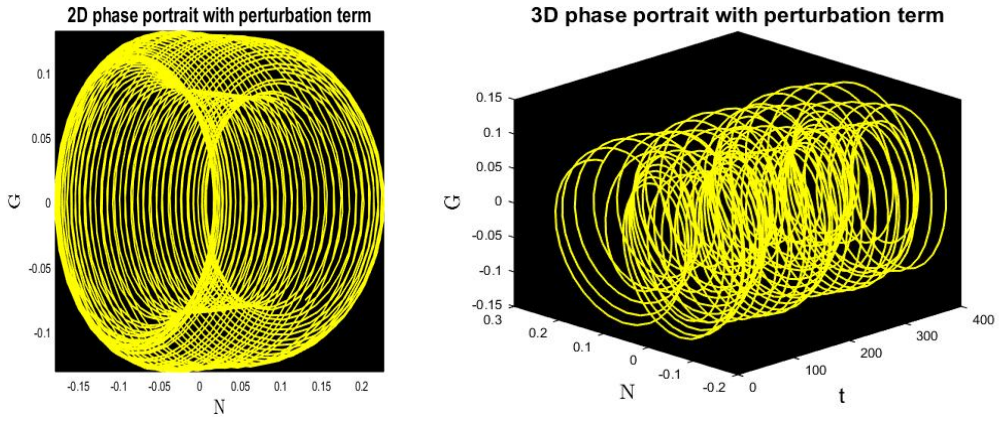

(a) (b)

Figure 5. Visualization of 2D and 3D chaotic dynamics with $\hat{\alpha} = 0.1$ and $\varepsilon = 0.25$.

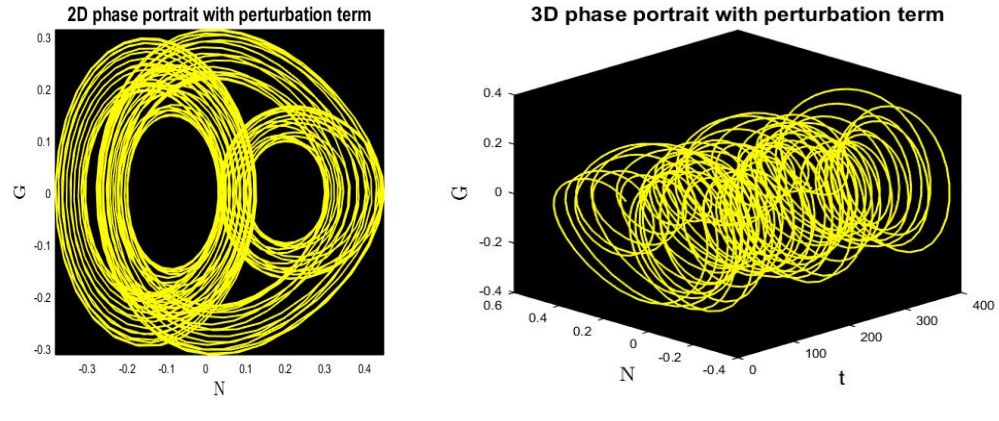

(a) (b)

Figure 6. Visualization of 2D and 3D chaotic dynamics with $\hat{\alpha} = 0.2$ and $\varepsilon = 0.25$.

5. Results and discussion

We have developed the exact solution for the generalized (3+1)-dimensional fractional q-deformed tanh-Gordon model using the SSET. This study presents an innovative approach through the utilization of the SSET and conducts comprehensive analyses of the dynamical system, bifurcation, chaotic analysis. To ensure the solutions are highly sensitive, look at the chaotic analysis of the ones that were obtained. Numerous wave solutions in the form of trigonometric and hyperbolic functions have been produced by the suggested method, these solutions are distinct and have important ramifications for mathematical physics. Plotting the multiple distinct architectures of the acquired solutions such as dark, bright, singular, and numerous periodic solutions is done to provide a physical explanation for the outcomes. Different sorts of solutions are obtained, such as bright, dark, kink, singular, and periodic solitons. In optical fibres and non-linear media, a bright soliton is a localized wave that keeps its shape while propagating and is distinguished by a peak over a zero or constant background. It frequently symbolizes energy or light pulses. A dark soliton, on the other hand, is important in optical and plasma physics and is characterized by a localized intensity dip in a continuous wave background. This type of soliton is usually seen in de-focusing nonlinear systems. They depict recurring wave shapes. The SSET along with Mathematica and MATLAB programming employing ode45 and RK4 techniques for phase plane analysis significantly improves computational efficiency. This is accomplished by efficiently managing complex calculations and symbolic operations that can surpass traditional numerical methods and speed up the analysis process. 3D plot of the fractional q-deformed equation's soliton solution for different deformation parameter q values. The plot shows the effect of the deformation on the soliton profile by showing how the soliton amplitude and width vary as q increases. The soliton solution's contour graphic illustrates the temporal and spatial evolution for fractional order. The graphic illustrates how fractional order affects the soliton's stability and propagation, while the outlines depict the soliton's wavefront. A two-dimensional graphic of the soliton solution with varying fractional order values.

Graphical representation

To gain a comprehensive knowledge of the physical properties of the solutions described, 3D, contour and 2D plots were generated by selecting appropriate parameter values (see Figures 7–11). These plots allow for a visual representation of how the solutions behave in different dimensions, which helps analyze their physical characteristics and behaviors. We recognize that previously displayed 2D and 3D graphs do not properly show the influence of fractional order. To address this, We added more charts showing how the solution profiles vary for various fractional parameter values. These comparison visualizations make possible a deeper physical understanding of the function of the fractional derivative in the system is made possible by these comparison visualizations, which make it clear how variations in fractional order affect the amplitude, and dynamics of the solutions. The fractional derivatives physically represent the impact of nonlocality spatial-temporal or long-range interactions, which can cause the solitons to exhibit more intricate and counterintuitive behavior.

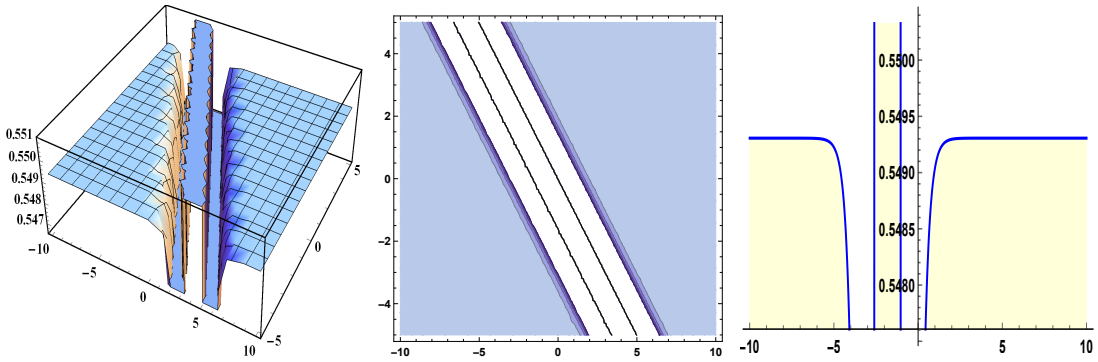

(a) 3D (b) Contour (c) 2D

Figure 7. Physical representation of $|R_4^{\pm}(x, y, z, t)|$, illustrate the solution of Eq (3.13) which is singular soliton when $\gamma = 0.5, C_1 = -1.5, \lambda = 1, \mu = 1, p = 2.2, q = 0.11, \rho_2 = 0.5, t = 1, z = 1$ and $\epsilon = 0.76$.

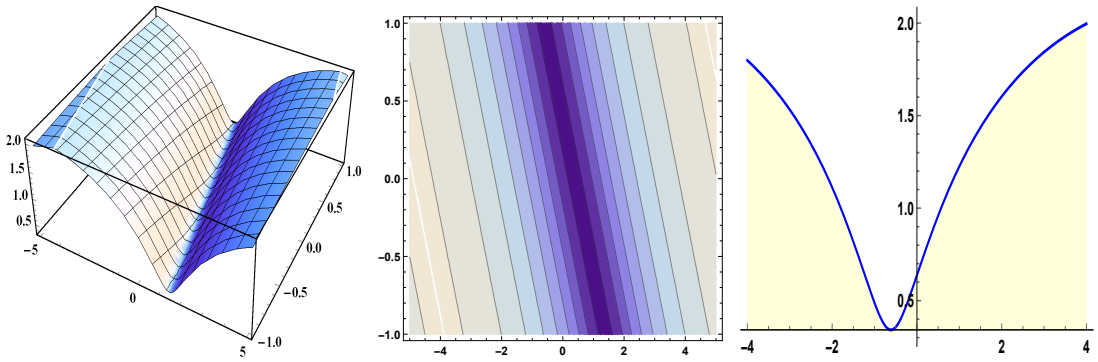

(a) 3D (b) Contour (c) 2D

Figure 8. Physical representation of $|R_7^{\pm}(x, y, z, t)|$ the dark soliton solution of Eq (3.16) when $\gamma = 0.5, C_1 = -0.04, \lambda = 1, \mu = 1, p = 0.52, q = 0.11, \rho_2 = -0.9, t = 1, z = 1$ and $\epsilon = 0.76$.

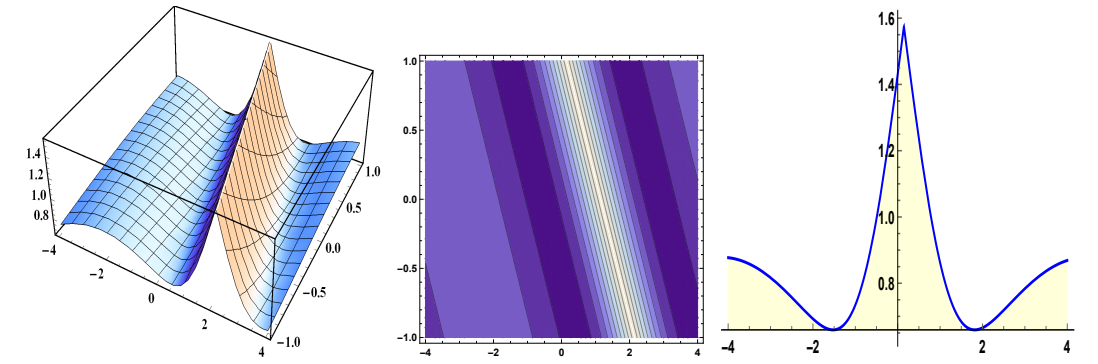

(a) 3D (b) Contour (c) 2D

Figure 9. Physical representation of $|R_8^{\pm}(x, y, z, t)|$the bright soliton of Eq (3.17) when $\gamma = 0.5, C_1 = -0.1, \lambda = 1, \mu = 1, p = 0.52, q = 0.11, \rho_2 = 0.5, t = 1, z = 1$ and $\epsilon = 0.76$.

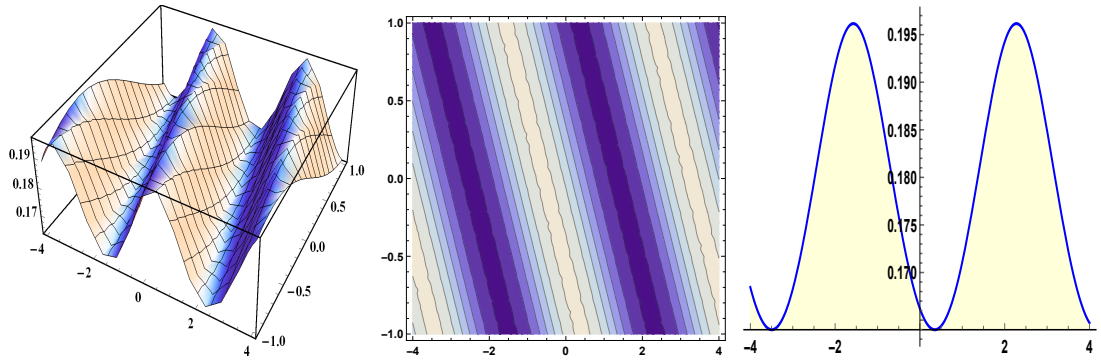

(a) 3D (b) Contour (c) 2D

Figure 10. Physical representation of $|R_9^{\pm}(x, y, z, t)|$,the solution of Eq (3.18) which is periodic soliton when $\gamma = 0.5, C_1 = -0.01, \lambda = 1, \mu = 1, p = 2.2, q = 1.11, \rho_2 = 0.32, t = 1, z = 1$ and $\epsilon = 0.76$.

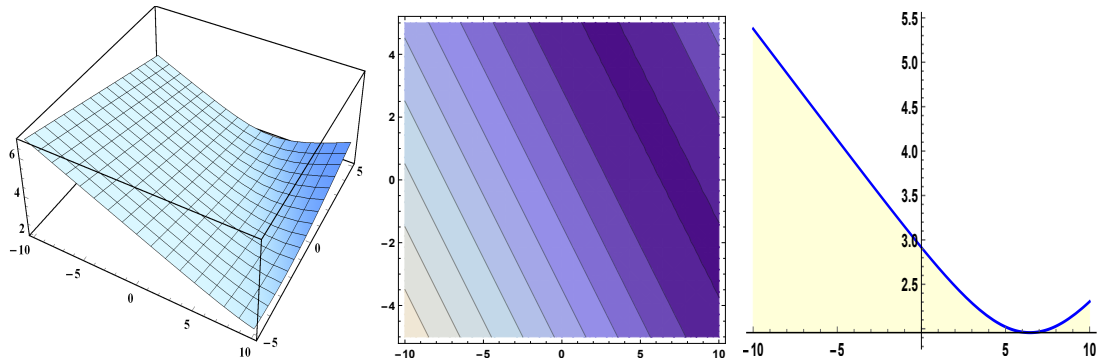

(a) 3D (b) Contour (c) 2D

Figure 11. Physical representation of $|R_{10}^{\pm}(x, y, z, t)|$ the smooth plane soliton of Eq (3.19) when $\gamma = 0.5, C_1 = -0.01, \lambda = 1, \mu = 1, p = 2.2, q = 1.11, \rho_2 = 0.32, t = 1, z = 1$ and $\epsilon = 0.76$.

6. Conclusions

A well-known fractional quantum equation that controls the propagation of nonlinear waves in a range of physical settings, including shallow water waves, optical fibres, and plasma physics, is the q-deformed fractional equation. This thorough study offers a thorough analytical and dynamic analysis of this problem. The governing equation has a set of new and precise solitary wave solutions. The analytical solutions were found using the SSET, which offered fresh perspectives on the intricate dynamics and nonlinear behavior present in the model under study. Graphical representations of the localized nature, characteristic structures, and amplitude profiles of these solitary wave solutions allow for a better understanding of the physics behind the model. In order to investigate bifurcations and chaotic behavior of the governing equation, we also used Galilean transformation to turn the ODE into a dynamical system. We used MATLAB to create graphical representations that improved our understanding of the dynamics of the system. Our work is creative and has the potential to produce

many new accomplishments that have not yet been discovered.

Author contributions

A. Naseem: Conceptualization, formal analysis, writing the original draft, review, software implementation and editing; R. Hussain: Formal analysis, software implementation, supervision, writing and review. All authors have read and approved the final version of the manuscript for publication.

Use of Generative-AI tools declaration

The authors declare that they have not used Artificial Intelligence (AI) tools in the creation of this article.

Conflict of interest

The authors declare that they have no competing interests.

References

1. S. Javed, A. Ali, J. Ahmad, R. Hussain, Study the dynamic behavior of bifurcation, chaos, time series analysis and soliton solutions to a Hirota model, *Opt. Quant. Electron.*, **55** (2023), 1114. https://doi.org/10.1007/s11082-023-05358-8
2. T. Rasool, R. Hussain, M. A. Al Sharif, W. Mahmoud, M. S. Osman, A variety of optical soliton solutions for the M-truncated Paraxial wave equation using Sardar-subequation technique, *Opt. Quant. Electron.*, **55** (2023), 396. https://doi.org/10.1007/s11082-023-04655-6
3. M. H. Rafiq, A. Jhangeer, N. Raza, The analysis of solitonic, super non linear, periodic, quasi periodic, bifurcation and chaotic patterns of perturbed Gerdjikov–Ivanov model with full nonlinearity, *Commun. Nonlinear Sci.*, **116** (2023), 106818. https://doi.org/10.1016/j.cnsns.2022.106818
4. D. Baleanu, A. Jajarmi, S. S. Sajjadi, J. H. Asad, The fractional features of a harmonic oscillator with position-dependent mass, *Commun. Theor. Phys.*, **72** (2020), 055002. https://doi.org/10.1088/1572-9494/ab7700
5. R. Hussain, A. Naseem, S. Javed, Analytical and numerical investigation for a new generalized q-deformed sinh-Gordon equation, *Opt. Quant. Electron.*, **56** (2024), 818. https://doi.org/10.1007/s11082-024-06624-z
6. M. N. Rafiq, H. Chen, Multiple interaction solutions, parameter analysis, chaotic phenomena and modulation instability for a (3+ 1)-dimensional Kudryashov–Sinelshchikov equation in ideal liquid with gas bubbles, *Nonlinear Dynam.*, 2024, 1–24.
7. A. Ali, J. Ahmad, S. Javed, Exact soliton solutions and stability analysis to (3+ 1)-dimensional nonlinear Schrödinger model, *Alex. Eng. J.*, **76** (2023), 747–756. https://doi.org/10.1016/j.aej.2023.06.067

8. S. Zhang, T. Xia, A generalized new auxiliary equation method and its applications to nonlinear partial differential equations, *Physics Lett. A*, **363** (2007), 356–360. https://doi.org/10.1016/j.physleta.2006.11.035
9. S. H. Strogatz, *Nonlinear dynamics and chaos: With applications to physics, biology, chemistry, and engineering*, CRC press, 2018.
10. B. B. Thomas, G. Betchewe, K. K. Victor, K. T. Crepin, On periodic wave solutions to (1+1)-dimensional nonlinear physical models using the sine-cosine method, *Acta Appl. Math.*, **110** (2010), 945–953. https://doi.org/10.1007/s10440-009-9487-4
11. A. M. Wazwaz, Two reliable methods for solving variants of the KdV equation with compact and noncompact structures, *Chaos Soliton. Fract.*, **28** (2006), 454–462. https://doi.org/10.1016/j.chaos.2005.06.004
12. E. Yomba, The modified extended Fan sub-equation method and its application to the (2+ 1)-dimensional Broer–Kaup–Kupershmidt equation, *Chaos Soliton. Fract.*, **27** (2006), 187–196. https://doi.org/10.1016/j.chaos.2005.03.021
13. J. H. He, X. H. Wu, Exp-function method for nonlinear wave equations, *Chaos Soliton. Fract.*, **30** (2006), 700–708. https://doi.org/10.1016/j.chaos.2006.03.020
14. M. A. Abdou, The extended sech method and its applications for solving nonlinear physical models, *Appl. Math. Comput.*, **190** (2007), 988–996. https://doi.org/10.1016/j.amc.2007.01.070
15. J. Zhang, X. Wei, Y. Lu, A generalized $(\frac{G'}{G})$-expansion method and its applications, *Phys. Lett. A*, **372** (2008), 3653–3658. https://doi.org/10.1016/j.physleta.2008.02.027
16. K. Hosseini, A. Bekir, R. Ansari, Exact solutions of nonlinear time-fractional Boussinesq equations using the $\exp(-\phi)$-expansion method, *Opt. Quant. Electron.*, **49** (2017), 1–11. https://doi.org/10.1007/s11082-017-0968-9
17. Y. Yıldırım, Optical solitons with Biswas–Arshed equation by F-expansion method, *Optik*, **227** (2021), 165788. https://doi.org/10.1016/j.ijleo.2020.165788
18. P. Capetillo, J. Hornewall, *Introduction to the Hirota direct method*, 2021.
19. V. Marchenko, *The inverse scattering problem and its application to NLPDE*, In Scattering, Academic Press, 2002, 1695–1706. https://doi.org/10.1016/B978-012613760-6/50094-2
20. M. Makaryan, *Generalized darboux transformation and nth*, Doctoral dissertation, California State University, Northridge,2016.
21. M. Khater, S. Anwar, K. U. Tariq, M. S. Mohamed, Some optical soliton solutions to the perturbed nonlinear Schrödinger equation by modified Khater method, *AIP Adv.*, **11** (2021). https://doi.org/10.1063/5.0038671
22. X. F. Yang, Z. C. Deng, Y. Wei, A Riccati-Bernoulli sub-ODE method for nonlinear partial differential equations and its application, *Adv. Differ. Equ.*, 2015, 1–17. https://doi.org/10.1186/s13662-015-0452-4
23. M. Younis, N. Cheemaa, S. A. Mahmood, S. T. Rizvi, On optical solitons: The chiral nonlinear Schrödinger equation with perturbation and Bohm potential, *Opt. Quant. Electron.*, **48** (2016), 1–14. https://doi.org/10.1007/s11082-016-0809-2

24. U. Aglietti, L. Griguolo, R. Jackiw, S. Y. Pi, D. Seminara, Anyons and chiral solitons on a line, *Phys. Rev. Lett.*, **77** (1996), 4406. https://doi.org/10.1103/PhysRevLett.77.4406
25. Y. He, Y. Kai, Wave structures, modulation instability analysis and chaotic behaviors to Kudryashov's equation with third-order dispersion, *Nonlinear Dynam.*, **112** (2024), 10355–10371. https://doi.org/10.1007/s11071-024-09635-3
26. Y. Kai, L. Huang, Dynamic properties, Gaussian soliton and chaotic behaviors of general Degasperis–Procesi model, *Nonlinear Dynam.*, **111** (2023), 8687–8700. https://doi.org/10.1007/s11071-023-08290-4
27. A. Nishino, Y. Umeno, M. Wadati, Chiral nonlinear Schrödinger equation, *Chaos Soliton. Fract.*, **9** (1998), 1063–1069. https://doi.org/10.1016/S0960-0779(97)00184-7
28. K. K. Ali, H. I. Alrebdi, N. A. Alsaif, A. H. Abdel-Aty, H. Eleuch, Analytical solutions for a new form of the generalized q-deformed sinh–gordon, *Symmetry*, **15** (2023), 470. https://doi.org/10.3390/sym15020470
29. K. K. Ali, W. G. Alharbi, Exploring unconventional optical soliton solutions for a novel $\mathfrak{q}$-deformed mathematical model, *AIMS Math.*, **9** (2024), 15202–15222. https://doi.org/10.3934/math.2024738
30. K. K. Ali, M. S. Mohamed, M. Maneea, Exploring optical soliton solutions of the time fractional q-deformed Sinh-Gordon equation using a semi-analytic method, *AIMS Math.*, **8** (2023), 27947–27968. https://doi.org/10.3934/math.20231429
31. K. K. Ali, Investigating novel optical soliton solutions for a generalized (3+1)-dimensional q-deformed equation, *Z. Angew. Math. Phys.*, **75** (2024), 208. https://doi.org/10.1007/s00033-024-02344-2
32. M. N. Rafiq, M. H. Rafiq, H. Alsaud, Chaotic response, multistability and new wave structures for the generalized coupled Whitham-Broer-Kaup-Boussinesq-Kupershmidt system with a novel methodology, *Chaos Soliton. Fract.*, **190** (2025), 115755. https://doi.org/10.1016/j.chaos.2024.115755
33. A. Jhangeer, N. Raza, A. Ejaz, M. H. Rafiq, D. Baleanu, Qualitative behavior and variant soliton profiles of the generalized P-type equation with its sensitivity visualization, *Alex. Eng. J.*, **104** (2024), 292–305. https://doi.org/10.1016/j.aej.2024.06.046
34. M. N. Rafiq, M. H. Rafiq, H. Alsaud, Diversity of soliton dynamics, positive multi-complexiton solutions and modulation instability for (3+1)-dimensional extended Kairat-X equation, *Mod. Phys. Lett. B*, 2025, 2550112.
35. M. N. Rafiq, M. H. Rafiq, H. Alsaud, New insights into the diversity of stochastic solutions and dynamical analysis for the complex cubic NLSE with δ-potential through Brownian process, *Commun. Theor. Phys.*, 2025.
36. Z. Li, J. Lyu, E. Hussain, Bifurcation, chaotic behaviors and solitary wave solutions for the fractional Twin-Core couplers with Kerr law non-linearity, *Sci. Rep.*, **14** (2024), 22616. https://doi.org/10.1038/s41598-024-74044-w
37. K. Zhang, J. Cao, Dynamic behavior and modulation instability of the generalized coupled fractional nonlinear Helmholtz equation with cubic–quintic term, *Open Phys.*, **23** (2025), 20250144. https://doi.org/10.1515/phys-2025-0144

38. K. Zhang, J. Cao, J. Lyu, Dynamic behavior and modulation instability for a generalized nonlinear Schrödinger equation with nonlocal nonlinearity, *Phys. Scripta*, **100** (2024), 015262. https://doi.org/10.1088/1402-4896/ad9cfa

AIMS Press